Rogozhina, I., Hagedoorn, J., Martinec, Z., Fleming, K., Soucek, O., Greve, R., Thomas, M. (2012): Effects of uncertainties in the geothermal heat flux distribution on the Greenland Ice Sheet: An assessment of existing heat flow models. - Journal of Geophysical Research, 117, F02025

DOI: 10.1029/2011JF002098

Effects of uncertainties in the geothermal heat flux distribution on the Greenland Ice Sheet: An assessment of existing heat flow models

I. Rogozhina,[1] J. M. Hagedoorn,[1] Z. Martinec,[2,3] K. Fleming,[1] O. Soucek,[3] R. Greve,[4] and M. Thomas[1,5]

Received 23 May 2011; revised 4 April 2012; accepted 10 April 2012; published 22 May 2012.

[1] This study analyzes the uncertainties in the models of the Greenland Ice Sheet (GIS) that arise from ill-constrained geothermal heat flux (GHF) distribution. Within the context of dynamic GIS modeling, we consider the following questions: (i) What is the significance of the differences between the existing GHF models for the GIS modeling studies? (ii) How well does the modeled GIS controlled by the GHF models agree with the observational data? (iii) What are the relative contributions of uncertainties in GHF and climate forcing to the misfit between the observed and modeled present-day GIS? The results of paleoclimatic simulations suggest that differences in the GHF models have a major effect on the history and resulting present-day state of the GIS. The ice sheet model controlled by any of these GHF forcings reproduces the observed GIS state to only a limited degree and fails to reproduce either the topography or the low basal temperatures measured in southern Greenland. By contrast, the simulation controlled by a simple spatially uniform GHF forcing results in a considerably better fit with the observations, raising questions about the use of the three GHF models within the framework of GIS modeling. Sensitivity tests reveal that the misfit between the modeled and measured temperatures in central Greenland is mostly due to inaccurate GHF and Wisconsin precipitation forcings. The failure of the ice sheet model in southern Greenland, however, is mainly caused by inaccuracies in the surface temperature forcing and the generally overestimated GHF values suggested by all GHF models.

Citation: Rogozhina, I., J. M. Hagedoorn, Z. Martinec, K. Fleming, O. Soucek, R. Greve, and M. Thomas (2012), Effects of uncertainties in the geothermal heat flux distribution on the Greenland Ice Sheet: An assessment of existing heat flow models, *J. Geophys. Res.*, *117*, F02025, doi:10.1029/2011JF002098.

1. Introduction

[2] Over the last decades, the basal thermal regimes of large ice sheets, ice caps and mountain glaciers have been the subject of intensive studies [e.g., *Brinkerhoff et al.*, 2011; *Chandler et al.*, 2006; *Gudmundsson and Raymond*, 2008; *Johnson and Fastook*, 2002; *Maxwell et al.*, 2008]. The thermodynamic state of basal ice layers determines, to a large extent, the overall dynamic behavior of grounded ice masses, especially by (i) the formation of basal temperate ice that undergoes enhanced deformation, and (ii) the process of basal melting, which controls sliding processes and most basal transport phenomena. In turn, the magnitude and distribution of geothermal heat flux (GHF) is one of the major uncertainties in understanding the basal thermal conditions of the Greenland and Antarctic Ice Sheets.

[3] Recent studies have revealed significant variability in the GHF distribution under ice sheets, controlled by regional variations in bedrock topography and composition, the thickness of the lithosphere and crustal heat production [e.g., *Bell*, 2008; *Fahnestock et al.*, 2001; *Fox Maule et al.*, 2005, 2009; *Smith et al.*, 2009; *van der Veen et al.*, 2007]. Valuable information about basal ice temperatures and temperature gradients has been obtained from a number of deep ice cores in Antarctica [e.g., *Augustin et al.*, 2004; *Barbante et al.*, 2006; *Jouzel et al.*, 1993, 1997; *Petit et al.*, 1999; *Sowers et al.*, 1993; *Watanabe et al.*, 2003]. The discovery of numerous subglacial lakes [e.g., *Bell*, 2008; *Smith et al.*, 2009] can potentially provide additional constraints on the basal thermal state of the Antarctic Ice Sheet [*Llubes et al.*, 2006; *Pattyn*, 2010]. In the Greenland region, only a

[1]Helmholtz Centre Potsdam, GFZ German Research Centre for Geosciences, Potsdam, Germany.
[2]Dublin Institute for Advanced Studies, Dublin, Ireland.
[3]Department of Geophysics, Faculty of Mathematics and Physics, Charles University, Prague, Czech Republic.
[4]Institute of Low Temperature Science, Hokkaido University, Sapporo, Japan.
[5]Institute of Meteorology, Free University Berlin, Berlin, Germany.

Corresponding author: I. Rogozhina, Helmholtz Centre Potsdam, GFZ German Research Centre for Geosciences, Telegrafenberg, D-14473 Potsdam, Germany. (valmont@gfz-potsdam.de)

0148-0227/12/2011JF002098

handful of deep ice cores exist [*Anderson et al.*, 2004; *Greenland Ice Core Project members*, 1993; *Alley et al.*, 1993; *Dahl-Jensen et al.*, 1998; *Dansgaard et al.*, 1993; *Johnsen et al.*, 2001; *Meese et al.*, 1994]. This limits the number of reliable heat flux and basal ice temperature estimates to only a few locations at the deep ice cores and some coastal drilling sites. Additional information on the basal thermal conditions of the Greenland Ice Sheet (GIS) was provided by *Fahnestock et al.* [2001] who revealed large regions of rapid basal melting in central Greenland using data from airborne ice-penetrating radar. These findings were supported by *Buchardt and Dahl-Jensen* [2007] who estimated high GHF values and basal melting rates at the location of NGRIP (North Greenland Ice Core Project) [*Anderson et al.*, 2004] using inverse modeling. Nevertheless, the GHF remains one of the least known boundary conditions required for the accurate modeling of the dynamics of the GIS and the understanding of its present-day thermal state.

[4] Most existing studies dealing with dynamic GIS models have the GHF spatially and temporally constant under the entire GIS, with different models employing values between 42 and 65 mW/m^2 [e.g., *Calov and Hutter*, 1996; *Greve*, 2000; *Huybrechts and de Wolde*, 1999; *Ritz et al.*, 1996]. While using temporally constant GHF forcing is well justified owing to the processes influencing GHF being slow in comparison to the time scales over which ice sheet dynamics are studied [*Ritz*, 1987], the effects of large- and small-scale spatial variations in GHF on the regional thermal state of the basal ice layers are non-negligible and must be taken into account.

[5] A number of studies have employed ice sheet models of different levels of complexity in order to tune GHF forcing and constrain basal thermal conditions at the locations of the deep ice cores and subglacial lakes [*Greve*, 2005; *Llubes et al.*, 2006; *Pattyn*, 2010; *Tarasov and Peltier*, 2003]. Although these studies provide a simple way of estimating GHF values in compliance with the existing measurements of basal ice temperatures, it remains unclear how the simplified assumptions within these models and a limited knowledge of past climate variations affect the resultant GHF values.

[6] The need for better knowledge of the GHF distribution has motivated several global and regional studies to develop GHF models using various types of data, such as seismic tomography, magnetic field observations, and the tectonic age and geological structure of the bedrock [e.g., *Fox Maule et al.*, 2005, 2009; *Pollack et al.*, 1993; *Pollard et al.*, 2005; *Shapiro and Ritzwoller*, 2004]. For the Greenland region, only three GHF models are available [*Fox Maule et al.*, 2009; *Pollack et al.*, 1993; *Shapiro and Ritzwoller*, 2004]. All of these are based on indirect calculations, with none constrained by direct measurements. Due to the different methods used, there are significant discrepancies between the resulting GHF maps, not only in terms of their spatial patterns across the extent of the GIS, but also in their mean values.

[7] In this study, we analyze the differences between three GHF models, namely the tectonic model of *Pollack et al.* [1993], the seismic model of *Shapiro and Ritzwoller* [2004] and the magnetic model of *Fox Maule et al.* [2009], and assess the significance of these differences within the context of dynamic GIS modeling. We focus particularly on the effects the differences between the GHF models have on modeled descriptions of the present-day and past GIS topography and thermal regime, using the polythermal ice sheet model SICOPOLIS [*Greve*, 1995, 1997a] to model large-scale GIS dynamics. We perform a series of paleoclimatic simulations of the GIS controlled by the three GHF models and compare the resulting modeled basal temperatures and vertical temperature profiles with the measured ones at the locations of the deep ice cores. A perfect agreement between the modeled and measured temperatures is unlikely to be obtained, not only because of inaccuracies in the GHF forcing, but also because of the many simplifying assumptions in the ice sheet model itself, as well as our limited knowledge of past climate variations. All of these factors are presumed to have a strong effect on the modeled thermal state of the ice sheet. Whereas we cannot accommodate all of the limitations of the modeling approach used, we attempt to estimate the relative contributions of major model inputs, namely GHF and past climate forcings, on the resulting basal temperatures and ice thicknesses. Finally, we report on the successes and failures of the GIS model controlled by each of the three GHF models in view of our knowledge of the thermal state of the present-day GIS.

2. Methodology and Input Data

2.1. Ice Sheet Model

[8] The ice sheet model SICOPOLIS [*Greve*, 1995, 1997a] is based on the shallow ice approximation (SIA) [*Hutter*, 1982, 1983; *Morland*, 1984] and the rheology of an incompressible, heat-conducting, power law fluid [see *Greve and Blatter*, 2009; *Paterson*, 1994]. It simulates the time-dependent extent, thickness, 3-D velocity, temperature distribution, water-content and age of grounded ice in response to external forcing.

[9] The complete set of field equations and boundary conditions employed by the SICOPOLIS model can be found in *Greve* [1995, 1997a]. Here, we only present the main prognostic equations for the case of the polythermal ice method (moisture-mixture approach).

[10] The equation for the ice thickness is given by

$$\frac{\partial H}{\partial t} = \frac{\partial (h-b)}{\partial t} = -\frac{\partial q_x}{\partial x} - \frac{\partial q_y}{\partial y} + a_s - a_b, \tag{1}$$

where x and y are the horizontal Cartesian coordinates, z is the vertical Cartesian coordinate defined as elevation above sea level, t is the time, h is the z-coordinate of the ice surface, b is the z-coordinate of the ice base (lithosphere surface), H is the ice thickness, q_x and q_y are the components of the horizontal mass flux, a_s is the accumulation-ablation function at the ice surface, a_b is the basal melting rate, and ρ is the density of ice.

[11] The equation for the bedrock response to changing ice loads is expressed as

$$\frac{\partial b}{\partial t} = -\frac{1}{\tau_\nu}\left[b - \left(b_0 - \frac{\rho}{\rho_a} H\right)\right], \tag{2}$$

where τ_ν is the time lag for the lithosphere response, b_0 is the position of b for the relaxed lithosphere surface without an ice load, and ρ_a is the density of the asthenosphere.

[12] The temperature equation for cold ice regions is

$$\frac{\partial T}{\partial t} + v_x \frac{\partial T}{\partial x} + v_y \frac{\partial T}{\partial y} + v_z \frac{\partial T}{\partial z} = \frac{1}{\rho c}\left[\frac{\partial}{\partial z}\left(\kappa \frac{\partial T}{\partial z}\right) + 2EA(T')f(\sigma)\sigma^2\right], \tag{3}$$

where T is the temperature, v_x, v_y, and v_z are the components of ice velocity, c is the specific heat of ice, κ is the heat conductivity of ice, E is the creep enhancement factor, $A(T')$ is the rate factor for cold ice, which is dependent upon the temperature below pressure-melting point (BPMP), $T' = T - T_{melt}$, where T is the temperature of the ice and T_{melt} is the temperature at the pressure melting point, and $f(\sigma)$ is the creep function for cold ice, dependent upon the effective shear stress σ.

[13] The water content in temperate ice regions is given by

$$\frac{\partial \omega}{\partial t} + v_x \frac{\partial \omega}{\partial x} + v_y \frac{\partial \omega}{\partial y} + v_z \frac{\partial \omega}{\partial z} = \frac{1}{\rho}\left[\frac{2}{L} EA_t(\omega) f_t(\sigma)\sigma^2 - D(\omega)\right] + CCC, \tag{4}$$

where ω is the water content (i.e., the mass fraction of water in the mixture), L is the latent heat of ice, $A_t(\omega)$ is the creep rate factor for temperate ice, $f_t(\sigma)$ is the creep function for temperate ice, $D(\omega)$ is the water drainage function, and CCC is the Clausius-Clapeyron correction.

[14] The age of cold (temperate) ice is expressed as

$$\frac{\partial A}{\partial t} + v_x \frac{\partial A}{\partial x} + v_y \frac{\partial A}{\partial y} + v_z \frac{\partial A}{\partial z} = 1 + D_A \frac{\partial^2 A}{\partial z^2}, \tag{5}$$

where A is the age of the ice and D_A is the numerical diffusivity, which is needed for reasons of numerical stability.

[15] The temperature equation for the lithosphere is given by

$$\frac{\partial T}{\partial t} + \frac{\partial b}{\partial t}\frac{\partial T}{\partial z} = \frac{\kappa_r}{\rho_r c_r}\frac{\partial^2 T}{\partial z^2}, \tag{6}$$

where κ_r is the heat conductivity of the lithosphere, ρ_r is the density of the lithosphere, and c_r is the specific heat of the lithosphere.

[16] Basal sliding is described by a Weertman-type sliding law (as in *Greve et al.* [1998]), modified to allow for submelt sliding as proposed by *Hindmarsh and Le Meur* [2001]:

$$\vec{v}_b(T'_b) = -\frac{C_b(T'_b)}{\rho g}\frac{|\vec{\tau}|^{p-1}}{P^q}, \tag{7}$$

where $\vec{v}_b$ is the basal-sliding velocity, $\vec{\tau}$ is the basal traction in the bed plane, g is the gravitational acceleration and $P = \rho g H$ is the overburden pressure. The stress and pressure exponents are chosen to be p = 3 and q = 2. The sliding coefficient C_b depends on the temperature BPMP, T'_b, via

$$C_b = C_b^0 e^{T'_b/\gamma}, \tag{8}$$

where $C_b^0 = 10^5 a^{-1}$ is the sliding coefficient at the pressure-melting point, and the constant $\gamma = 1°\mathrm{C}$.

[17] External forcing entering the boundary conditions is specified by: (i) the mean annual air temperature and amplitude of the seasonal temperature changes, (ii) the surface mass balance, i.e., precipitation minus evaporation and ablation, (iii) the global sea level, and (iv) the geothermal heat flux.

[18] Here, we only present the thermal boundary conditions, which are relevant to the present study (for details, see *Greve* [1997a]). At the free surface it is given by

$$T = T^s(x, y, t), \tag{9}$$

where T^s is the temperature prescribed by the surface temperature forcing.

[19] The boundary conditions at the cold ice base are given by

$$T = T_r^s(x, y, t), \tag{10a}$$

$$\kappa \frac{\partial T}{\partial z} - \kappa_r \frac{\partial T_r^s}{\partial z} = -(v_b)_x \sigma_{xz} - (v_b)_y \sigma_{yz}, \tag{10b}$$

where T_r^s is the temperature at the top of the thermal lithosphere layer (bedrock), κ is the heat conductivity of the ice, $(v_b)_x$ and $(v_b)_y$ are the components of the basal-sliding velocity given in (7), and σ_{xz} and σ_{yz} are the components of the stress tensor.

[20] Boundary conditions at the temperate ice base overlain by a temperate ice layer are as follows

$$T = T_r^s(x, y, t) = T^*, \tag{11a}$$

$$a_b = \frac{1}{\rho L}\left(\kappa\beta - \kappa_r \frac{\partial T_r^s}{\partial z} + (v_b)_x \sigma_{xz} + (v_b)_y \sigma_{yz}\right), \tag{11b}$$

where T^* is the pressure-melting point of the ice, and β is the Clausius-Clapeyron gradient.

[21] Boundary conditions at the temperate ice base (not overlain by a temperate ice layer) are the following

$$T = T_r^s(x, y, t) = T^*, \tag{12a}$$

$$a_b = \frac{1}{\rho L}\left(\kappa \frac{\partial T}{\partial z} - \kappa_r \frac{\partial T_r^s}{\partial z} + (v_b)_x \sigma_{xz} + (v_b)_y \sigma_{yz}\right). \tag{12b}$$

[22] The thermal boundary condition at the base of the thermal lithosphere layer is given by

$$\kappa_r \frac{\partial T_r^b}{\partial z} = -Q_{GHF}, \tag{13}$$

where T_r^b is the temperature at the base of the thermal lithosphere layer (bedrock) situated at the depth H_r below the ice base (see Table 1), and Q_{GHF} is the GHF forcing.

[23] The thermomechanical coupling is described by the temperature-dependent rate factor, $A(T')$ [*Greve et al.*, 1998]. The isostatic adjustment of the lithosphere to the changing ice load (equation (2)) is modeled by the local-lithosphere-relaxing-asthenosphere approach with a relaxation time $\tau_\nu = 3000$ years (for more details, see *Greve* [2001] and *Le Meur and Huybrechts* [1996]). Surface melting is parameterized by the degree-day method [*Reeh*, 1991] and the semi-analytical solution for the positive-degree day integral [*Calov and Greve*, 2005]. The positive degree day factors are identical to those used by *Greve* [2005].

[24] The four main paleoclimatic simulations described in sections 3.1 and 3.2 employ a horizontal grid spacing of 10 km by 10 km, corresponding to 165 (east-west) by 281 (north-south) grid points in the stereographic plane, whereas

Table 1. Standard Physical Quantities Used for the Simulations in This Study

Quantity	Value
Density of ice, ρ	910 kg m^{-3}
Specific heat of ice, c	(146.3 + 7.253 T [K]) J kg^{-1} K^{-1}
Heat conductivity of ice, κ	9.828e$^{-0.0057T\ [K]}$ W m^{-1} K^{-1}
Latent heat of ice, L	335 kJ kg^{-1}
Clausius-Clapeyron gradient, β	8.7 $\times$ 10^{-4} K m^{-1}
Density $\times$ specific heat of the lithosphere, $\rho_r c_r$	2000 kJ m^{-3} K^{-1}
Heat conductivity of the lithosphere, κ_r	2 W m^{-1} K^{-1}
Thickness of the upper lithosphere layer, H_r	5 km
Time lag for lithosphere response, τ_ν	3000 years
Density of the asthenosphere, ρ_a	3300 kg m^{-3}

the sensitivity tests discussed in sections 4.1 and 4.2 have been carried out using a horizontal grid spacing of 20 km by 20 km, corresponding to 83 (east-west) by 141 (north-south) grid points in the stereographic plane. For the cold ice layers, 81 grid points in the vertical direction are mapped to [0, 1] intervals using the σ-transformation, such that $z = 0$ indicates the ice-bedrock boundary and $z = 1$ is the free ice surface [*Greve*, 1995]. The equations for the temperate basal layer, if present, and the bedrock are each solved for 11 equidistant grid points in the vertical direction. The standard physical quantities used for the paleoclimatic simulations are given in Table 1.

[25] The enhancement factor E is coupled to the accumulation time $t_{acc} = t - A$ which denotes the moment when an ice particle has been deposited on the surface of the ice sheet:

$$E = \begin{cases} 3, & t_{acc} < -132 \\ 1, & -132 \le t_{acc} < -114.5 \\ 3, & -114.5 \le t_{acc} < -11 \\ 1, & t_{acc} \ge -11 \end{cases}, \qquad (14)$$

where the age of the ice, A, the time, t, and the accumulation time, t_{acc}, are given in thousands of years (kyr), $t_{acc} < -132$ kyr means that the ice particle was deposited during the pre-Eemian period, $-132 \le t_{acc} < -114.5$ during the Eemian period, $-114.5 \le t_{acc} < -11$ during the Wisconsin period, and $t_{acc} \ge -11$ during the Holocene period.

[26] Initial conditions are provided by spin-up simulations from 250 to 150 kyr before present (BP) with different GHF distributions (see section 2.3). The spin-up simulations start with the present-day surface and bedrock topographies [*Layberry and Bamber*, 2001] as the initial state (i.e, an ice-covered initial state). The temperature of the initial ice body is uniformly set equal to -10°C and the initial age of the ice is set to 15 kyr [*Greve*, 1997b].

2.2. Climate Forcing

[27] The components of climate forcing are taken to be identical to those used by *Greve* [2005] with the exception of time-dependent factors describing air temperature variations over time, termed the glacial index $g(t)$, which in this work are based on the GRIP (Greenland Ice Core Project) ice core record reaching back to 250 kyr BP [*Greenland Ice Core Project Members*, 1993]. Climate forcing is constructed based on the present-day and Last Glacial Maximum (LGM, 21 kyr BP) distributions of precipitation and surface temperatures. The LGM temperature anomaly fields, ΔT_{ma_LGM} and ΔT_{mj_LGM}, and the LGM precipitation rates, P_{ma_LGM}, are provided by the atmospheric general circulation model UKMO [*Hewitt and Mitchell*, 1997] and corrected for temperature changes due to varying ice-surface elevation [*Greve*, 2005]. The glacial index $g(t)$ is employed to scale the precipitation and surface-temperature fields between the present-day and LGM climatic conditions. It is defined such that $g(t) = 1$ denotes LGM conditions, while $g(t) = 0$ corresponds to the present-day climatic conditions.

[28] The mean annual and July (summer) surface temperatures are parameterized by

$$T_{ma}(\theta, \varphi, t) = T_{ma\_present}(\theta, \varphi) + g(t) \cdot \Delta T_{ma\_LGM}(\theta, \varphi) \qquad (15a)$$

$$T_{mj}(\theta, \varphi, t) = T_{mj\_present}(\theta, \varphi) + g(t) \cdot \Delta T_{mj\_LGM}(\theta, \varphi), \qquad (15b)$$

where ΔT_{ma_LGM} and ΔT_{mj_LGM} are the mean annual and mean July LGM temperature anomalies, respectively, and θ and ϕ are latitude and longitude, respectively.

[29] The present-day surface temperatures, $T_{ma\_present}$ and $T_{mj\_present}$, are based on the parameterization by *Ritz et al.* [1996], fitting the observed present-day temperature fields.

[30] Monthly temperatures are calculated assuming a sinusoidal annual cycle, given by

$$T_{mm}(\theta, \varphi, t, n) = T_{ma}(\theta, \varphi, t) + \sin\left(\frac{(n-4)}{6}\pi\right) \cdot (T_{mj}(\theta, \varphi, t) - T_{ma}(\theta, \varphi, t)), \qquad (16)$$

where n = [1, …, 12] is the number of the month.

[31] Mean annual precipitation rates are computed as

$$P_{ma}(\theta, \varphi, t) = P_{ma\_present}(\theta, \varphi) \cdot (\Delta P_{ma\_LGM}(\theta, \varphi))^{-g(t)}, \qquad (17)$$

where $\Delta P_{ma\_LGM}(\theta, \varphi) = P_{ma\_LGM}(\theta, \varphi)/P_{ma\_present}(\theta, \varphi)$ is the LGM anomaly of the rate of precipitation.

[32] The present-day mean annual precipitation rates $P_{ma\_present}$ are based on the digitized accumulation map of *Calanca et al.* [2000]. Mean monthly precipitation rates are assumed to be equal to the mean annual rates and are converted into snowfall based on the relationship given by *Marsiat* [1994]:

$$S_{mm}(\theta, \varphi, t, n) = P_{ma}(\theta, \varphi, t) \cdot \begin{cases} 0, & T_{mm}(\theta, \varphi, t, n) \ge T_{rain} \\ \dfrac{T_{rain} - T_{mm}(\theta, \varphi, t, n)}{T_{rain} - T_{snow}}, & T_{snow} \le T_{mm}(\theta, \varphi, t, n) \le T_{rain} \\ 1, & T_{mm}(\theta, \varphi, t, n) \le T_{snow} \end{cases}, \qquad (18)$$

where $T_{snow} = -10$°C and $T_{rain} = +7$°C.

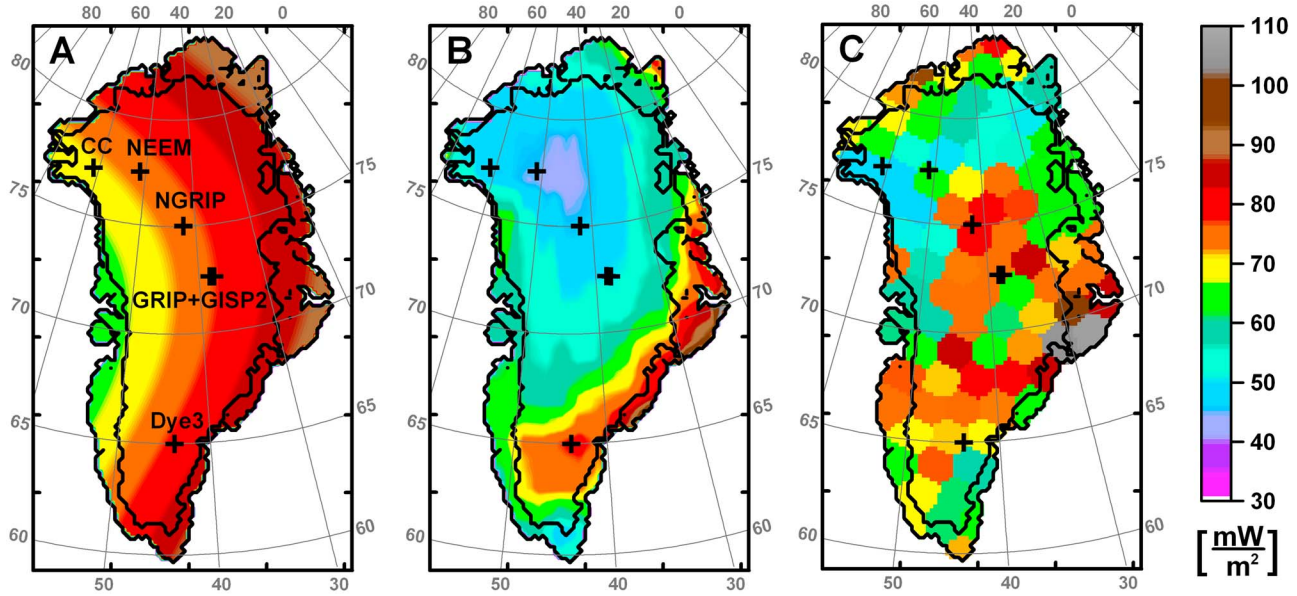

Figure 1. The GHF models used in this work as input for modeling the GIS evolution [mW/m^2]. (a) The tectonic model of *Pollack et al.* [1993]; (b) The seismic model of *Shapiro and Ritzwoller* [2004]; (c) The magnetic model of *Fox Maule et al.* [2009]. Black boundaries indicate the present-day coastline and area covered by the GIS. The black crosses are the locations of deep ice cores.

2.3. Geothermal Heat Flux Models

[33] The first GHF model considered in this study is the tectonic model of *Pollack et al.* [1993] (Figure 1a), which is based on the premise that similar geological units should display similar heat flow. The authors compiled heat flow observations from around the world and devised 21 categories (9 for continental lithosphere) of different tectonothermal ages and geological characteristics (geological units). The mean heat flow values based on the measured GHF values were calculated using an areal weighting of all grid elements with the same geological characteristic, and then assigned to the appropriate geological unit. The final global distribution of GHF was represented by a spherical harmonic expansion up to degree and order 12. The weakness of the model is its crude resolution (>1000 km) smoothing out the regional patterns of the resultant GHF distribution, and the poor knowledge of the geological structure under the GIS.

[34] The second GHF model is the seismic model of *Shapiro and Ritzwoller* [2004] (Figure 1b), which is derived from a 3-D seismic tomography model of the crust and upper mantle and the assumption of structural analogies between well-studied and unsurveyed regions. The model is based on the fact that there is a strong correlation between seismic tomography and mantle temperature. The weakness of the model is the assumption that crustal radioactive heat production is similar in regions with similar crustal structures. The spatial resolution of the model is 2° × 2° (2° being equal to 100–150 km at the latitudes of Greenland) [*Shapiro and Ritzwoller*, 2002].

[35] The third GHF model is the magnetic model of *Fox Maule et al.* [2009] (Figure 1c) which uses high-quality magnetic field data derived from the Ørsted, CHAMP and SAC-C satellite missions to map remnant crustal magnetization. This allowed the authors to first estimate the thickness of the magnetic crust and then determine the GHF values. Their thermal model of the crust is based on the assumption that the lower boundary of the magnetic crust coincides with the Curie isotherm. The authors considered a 4-layer model of crustal thermal conductivity and heat production. However, the method employs several simplifying assumptions, most importantly, it neglects variability in crustal radioactive heat production with respect to lithology. The GHF values are averaged over rhomb-shaped cells with areas of thousands of square kilometers (a few hundred kilometers in extent).

[36] In addition to the three GHF models, we employ as input to the ice sheet modeling a spatially uniform GHF forcing of 63 mW/m^2, which is the mean of the seismic and magnetic GHF values averaged over the Greenland region.

3. Results

3.1. The Influence of GHF Forcing on the GIS History

[37] We now examine the long-term effect of different GHF forcings on the evolution of basal temperatures and GIS volume during the last 150 kyr. For this purpose, we conduct a series of paleoclimatic simulations, which we designate as TRS (Tectonic Regionalization Simulation), STS (Seismic Tomography Simulation), MDS (Magnetic Data Simulation) and U63S (Uniform 63 mW/m^2 Simulation), controlled by the tectonic, seismic, magnetic and spatially uniform GHF fields (see section 2.3), respectively. In all cases, the heat flux is constant over time. These simulations are driven by the same time-dependent climate forcing, which is based on the ice surface temperature history inferred from the GRIP ice core record (Figure 2a; in addition see section 2.2).

[38] It should be noted that after the initialization procedure (approximately 100 kyr), the influence of the choice of initial state (see section 2.1) on the modeled GIS and its

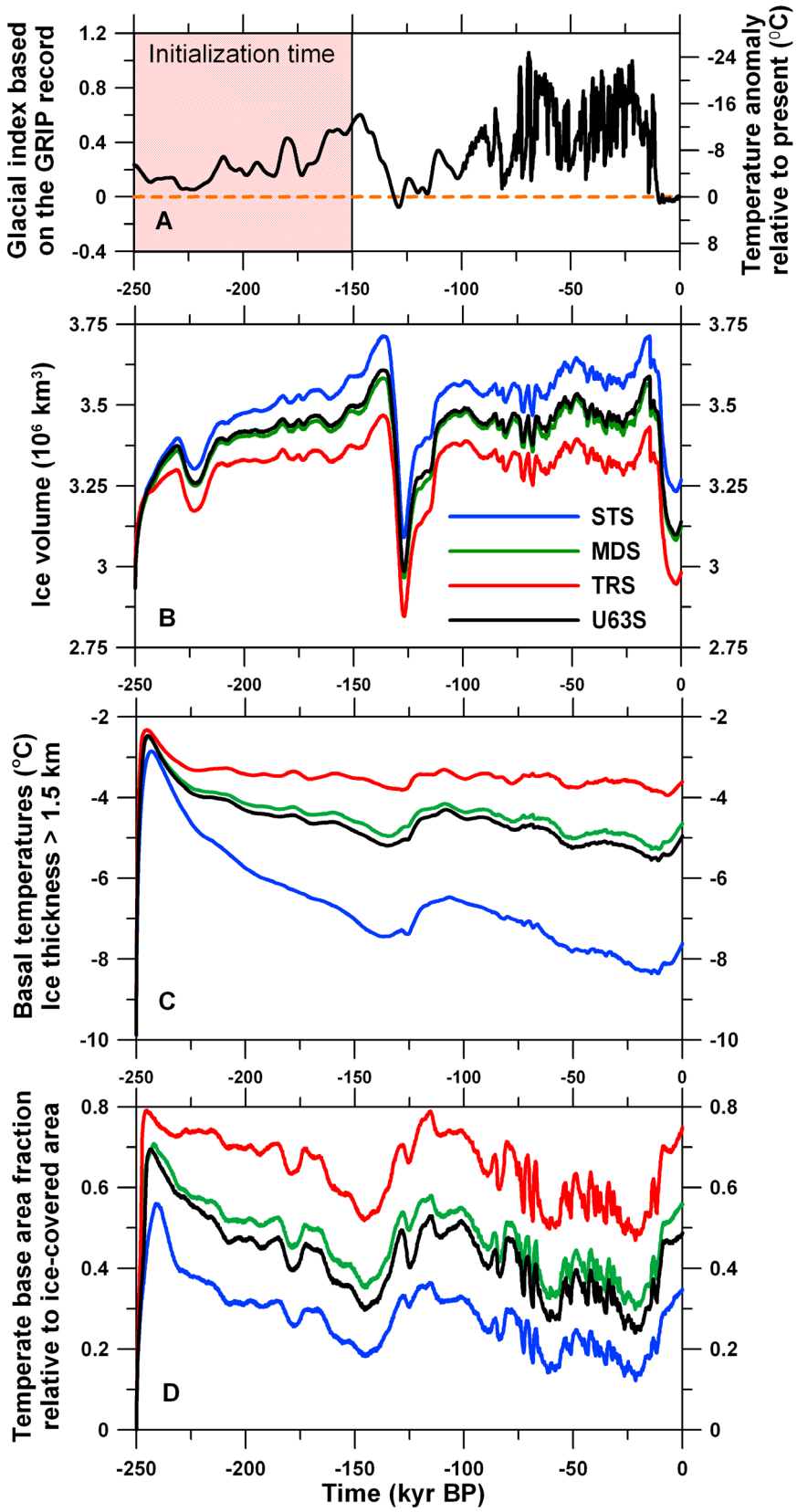

Figure 2. Response of the GIS model to the different GHF inputs and temporal variations in climatic conditions. (a) Time-dependent component (glacial index) of the climate forcing based on the GRIP ice core record [*Dansgaard et al.*, 1993]. The first 100 kyr are required to initialize the GIS model; (b) GIS volume; (c) Basal temperatures averaged over the area where the ice thickness is greater than 1.5 km; (d) Temperate base area with nonzero basal melting relative to the total GIS-covered area at each time slice.

thermal state is insignificant, as demonstrated by *Rogozhina et al.* [2011].

[39] In Figures 2b–2d, we show the response of the evolving GIS to the different GHF inputs by comparing the modeled evolutions of ice volume, mean basal temperature averaged over the area with ice thicknesses over 1.5 km, and temperate basal area relative to the total ice-covered area. The highest basal temperature, largest temperate base coverage and lowest ice volume over the course of the whole modeled GIS history result from the TRS (Figure 2, red curves) as a consequence of the higher heat flux relative to the GHF forcing employed by the other simulations.

[40] The present-day volumes from the STS, MDS and U63S (Figure 2b, blue, green and black curves, respectively) are 10%, 4.6% and 5.25% larger, respectively, than that from the TRS (Figure 2b, red curve). In general, despite the same climate forcing driving these simulations, the use of different GHF models results in different scenarios of the history of the GIS and its thermal regime. For example, during the LGM (21 kyr BP), the total ice volumes resulting from the STS, MDS and U63S are 8.6%, 4.1% and 5.1% larger, respectively, than that from the TRS.

[41] The TRS arrives at temperate basal conditions over 75% of the modeled present-day ice-covered area (Figure 2d, red curve; see also section 3.2 and Figure 4a), with the lowest temperate basal coverage (48%) during the LGM, whereas the highest temperate basal coverage (79%) is reached shortly after the Eemian interglacial. The temperate basal coverages resulting from the STS, MDS and U63S are about 40%, 19% and 26% smaller, respectively, throughout the modeled history.

[42] A relatively small difference of about 1°C between the mean basal temperatures computed by the TRS (Figure 2c, red curve) and MDS (Figure 2c, green curve) can be explained by the presence of large temperate base areas with basal ice at the pressure-melting point in both modeled GISs (Figure 2d; see also section 3.2 and Figures 4a and 4c). The present-day basal conditions in the inland part of the GIS computed by the STS (Figure 2c, blue curve) are by comparison 3°C to 4°C colder, indicating a major difference in its thermodynamic state relative to the other two modeled ice sheets.

[43] The evolution of the basal thermal regime and ice volume resulting from the U63S (Figures 2b–2d, black curves) shows a surprising similarity with the results from the MDS throughout the modeled history, despite it having GHF values 5–20 mW/m^2 lower in the central and southern inland areas and 5–15 mW/m^2 higher in the northern area compared to the magnetic GHF model (see Figure 1c). The basal temperatures produced by the U63S are slightly lower (from 0.1°C during the post-Eemian buildup to 0.3°C during the Holocene meltdown of the GIS) when compared to the MDS results, with the temperate ice area being 2–8% smaller and the GIS volume being slightly larger. Overall, the effects of the differences between the uniform and magnetic GHF models on the analyzed quantities of the modeled GIS are, however, minor, compared to the effects of the differences between the tectonic, seismic and magnetic GHF models.

[44] Figure 2c shows that the amplitudes of basal temperature changes throughout the glacial-interglacial period are smaller for the simulations with higher basal temperatures than for those with lower basal temperatures. Indeed, during the last 150 kyr, the basal conditions associated with the TRS vary in temperature by only 0.64°C, whereas the variations according to the MDS, U63S and STS amount to 1.13°C, 1.26°C and 1.9°C, respectively.

3.2. Modeled Present-Day GIS Versus Observations

[45] In this section, we examine the effects of the different GHF forcings integrated over the GIS history on the modeled present-day topography and ice temperature distribution, and compare the modeled and observed ice thicknesses and temperatures at the locations of the ice cores, where direct measurements are available.

[46] In Figure 3 the differences between the modeled and observed present-day ice thicknesses [*Bamber et al.*, 2001; *Layberry and Bamber*, 2001] are presented. The first observation is that all simulations produce significant discrepancies between the modeled and observed thicknesses, exceeding 1 km at the margins of the GIS and in two large areas in the most northern and eastern parts of Greenland. These misfits can be partly explained by the oversimplified treatment of temporal climate variations and ice sheet margin dynamics, which are responsible for the shape of the ice sheet's boundaries. Furthermore, the modeled ice dynamics in ice margin areas and in those areas with large horizontal gradients of bedrock and surface elevations (such as, for example, mountainous regions in eastern Greenland) suffer from the fundamental limitations of the SIA-based model used in our simulations [*Bueler et al.*, 2005; *Greve*, 1995]. At the same time, the analysis of GHF distribution in the mountainous and marginal regions is associated with higher uncertainties due to the strong influence of small- and large-scale variations in bedrock topography on the GHF values [*van der Veen et al.*, 2007]. This calls for higher-resolution estimations of the GHF distribution and far more sophisticated ice-flow models [e.g., *Brinkerhoff et al.*, 2011; *Goldberg and Sergienko*, 2011]. For these reasons, in this study, we focus on the effects of GHF on the inland GIS, excluding ice margin regions from further discussion.

[47] We can observe that all four simulations equally fail to reproduce the observed ice thicknesses in southern Greenland. On the western side of the southern GIS, the discrepancies between the observed and modeled thicknesses vary between 100 and 300 m, whereas the misfit reaches 400 to 600 m on the eastern side, including the location of the Dye 3 ice core. Another general tendency revealed by all four simulations is that the northeastern part of the GIS is always too thick and the northwestern part of the GIS is always too thin when compared with observations.

[48] The present-day GIS resulting from the TRS is generally too thin, with the exception of its central eastern and central western parts (Figure 3a). All along the divide the ice thicknesses are between 100 and 400 m too small compared to the observed ones. By contrast, northern and central parts of the GIS computed by the STS (Figure 3b) are 200 to 300 m too thick. Good agreement between the GIS thicknesses from the U63S and the MDS, which is only violated in central northern Greenland, again points out that the effects of the uniform and magnetic GHF forcings on the

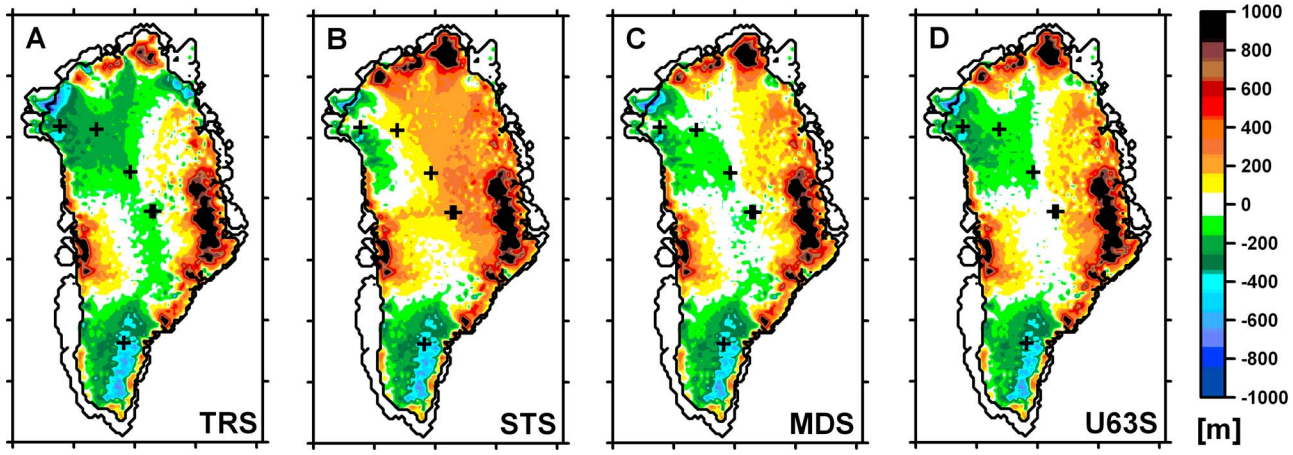

Figure 3. Differences between modeled and observed present-day ice thicknesses (meters) as a function of the employed GHF input. (a) TRS-observed, (b) STS-observed, (c) MDS-observed, and (d) U63S-observed. Black borders indicate the present-day modeled coastlines and margins of ice-covered areas. Locations of the boreholes (GRIP + GISP2, NGRIP, NEEM, CC and Dye 3) are marked by black crosses (see Figure 1).

modeled GIS are very similar (see section 3.1). In the north, the U63S produces 100–150 m too-thin ice relative to the observed GIS, whereas the MDS provides very good agreement with the observations in this region. In the central area close to the GRIP and GISP2 (Greenland Ice core Project two) ice cores, the GIS computed by the MDS is slightly thinner than that from the U63S. Among the four runs, the MDS provides the best fit to the divide thicknesses of the present-day GIS, with maximum discrepancies from the observed values not exceeding 50 m (except for the southern Greenland area).

[49] The present-day basal temperatures BPMP (below pressure-melting point, see section 2.1), T', computed by the four simulations are shown in Figure 4. As already indicated by the comparison between the observed and modeled ice thicknesses, the largest discrepancies can be expected in the southern part of the GIS. The TRS and STS suggest that most of the basal ice in the southern GIS, including the location of the Dye 3 station, is close to or at the pressure-melting point (Figures 4a and 4b). The other two simulations produce slightly lower basal temperatures BPMP, but again, these are very close to the pressure melting point, with the location of the Dye 3 site still lying at the margin of the cold-ice area surrounding the southern dome (Figures 4c and 4d). In reality, however, a large part of the southern GIS and the Dye 3 site itself should have a cold base in compliance with the extremely low basal temperature values observed at the Dye 3 site (−13.22°C; measured basal temperatures, T, can be found in Table 2).

[50] Comparing the present-day basal temperatures BPMP derived from the transient simulations reveals that the TRS produces higher temperatures overall than the other three runs, as already suggested by the analysis of the basal temperature evolution (see section 3.1). According to the TRS, most of the basal ice is close to the pressure-melting point and basal temperatures, T, at all ice core locations are too high compared to the observed values, with the only exception being the NGRIP site, where this simulation gives a good fit to the observed temperate basal conditions. Hence, the modeled basal temperature at NEEM (North Greenland Eemian Ice Drilling) is at the pressure-melting point as opposed to the observed non-temperate basal conditions, while basal ice at the GRIP, GISP2 and CC (Camp Century) sites has the highest temperatures relative to the results of the other simulations and is about 6°C too high compared to the observations.

[51] By contrast, the STS produces the lowest basal temperatures BPMP, T', and the smallest temperate ice area among the four runs. With the exception of the marginal areas, basal temperatures BPMP computed by the STS lie within the range of −4.5°C and −11°C over most of the northern and central parts of the present-day GIS (Figure 4b). The modeled basal temperatures, T, at the locations of the GRIP, GISP2 and NGRIP stations are 3.2°C, 2.6°C and 6.1°C, respectively, too low in comparison to the observed values. The computed basal temperatures at the CC and NEEM sites are both in agreement with the available data (see Table 2).

[52] The basal temperatures, T, from the MDS are about 5°C too high in the area of the GRIP and GISP2 stations (Table 2), but are close to the observed values at the NGRIP and CC and in agreement with the cold-ice conditions observed at NEEM. The MDS produces a very large temperate base area (Figure 4c) occupying more than 56% of the present-day GIS-covered territory, whereas large non-temperate areas are spread over most of the northern GIS and around the central and southern summits.

[53] The U63S produces the best agreement of the four runs with the observed basal temperatures at the locations of GRIP, GISP2 and Dye 3. It gives a temperature slightly below the pressure-melting point at the NGRIP base and a cold ice base at NEEM, in agreement with observations, with only the CC site having temperature that is too high, by 4.5°C. Although the modeled basal temperature at the Dye 3

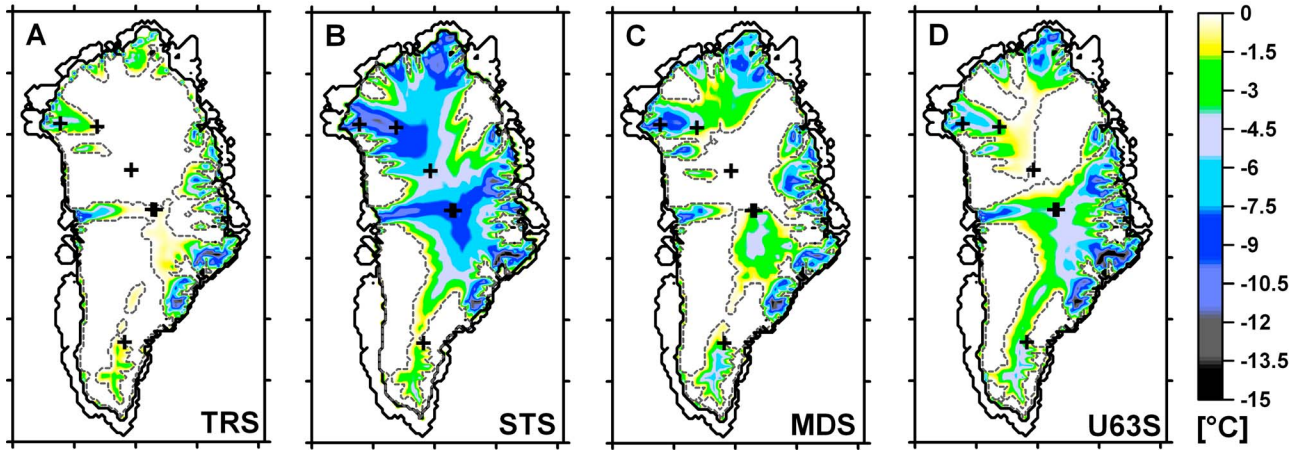

Figure 4. Basal temperatures BPMP (°C) computed using the (a) TRS, (b) STS, (c) MDS, and (d) U63S. Gray dashed lines indicate the boundaries of the modeled temperate base. Black borders indicate the present-day modeled coastlines and margins of ice-covered areas. Locations of the boreholes (GRIP + GISP2, NGRIP, NEEM, CC and Dye 3) are marked by black crosses (see Figure 1).

location is still unrealistically high, the cold-ice area around the southern dome predicted by the U63S is the largest relative to the results of the other three runs.

[54] In agreement with the existing data and estimations [*Fahnestock et al.*, 2001; *Grinsted and Dahl-Jensen*, 2002; *Dahl-Jensen et al.*, 2003; *Anderson et al.*, 2004; *Buchardt and Dahl-Jensen*, 2007], both the MDS and U63S suggest a temperate ice base in the present-day central-northern GIS.

[55] In Figure 5, we present modeled versus measured temperatures, *T*, at the locations of the GISP2, GRIP, NGRIP and Dye 3 ice cores (see Figure 1 for their locations) [*Clow et al.*, 1996; *Cuffey et al.*, 1995; *Johnsen et al.*, 1995] and differences between modeled and measured temperature profiles at the locations of GISP2 and GRIP. The temperature profiles from the U63S show the best agreement with the measured profiles from GRIP and GISP2, although the modeled temperatures of the uppermost ice layers are slightly too low. Below 400 m ice elevation (above the bedrock), however, the computed profiles diverge from the measured ones and arrive at 1.6°C and 2.2°C too-high temperatures at the ice sheet base as compared to the measurements at GRIP and GISP2, respectively (Figures 5f and 5e, black curves). The profiles resulting from the MDS and especially TRS show too-high temperatures between the ice base and 2000 m elevation above the bedrock, with the misfit increasing with depth and the discrepancies reaching 5°C to 6.5°C at the bases of the GRIP and GISP2 boreholes (Figures 5f and 5e, green and orange curves). The STS produces too-low temperatures all along the two profiles, being 1.6°C too-low at the surface due to the lapse rate (0.79°C per 100 m) and about 3°C too-low at the base (Figures 5e and 5f, gray curves). The ice at the locations of these two drill sites is also 200 m too thick compared to the measured values (Figures 5a and 5b). All modeled results show significant differences with respect to the observed vertical temperature gradients at the base of the Summit region.

[56] At the NGRIP site (Figure 5c), the STS produces ice almost 200 m thicker, with the surface and basal temperatures being 1.5°C and 6.1°C lower than observed. By contrast, the modeled ice thicknesses, and surface and basal temperatures resulting from the other three simulations agree well with the observed values at this location.

[57] Finally, at the Dye 3 location (Figure 5d), all modeled temperature profiles closely coincide with each other, although the temperatures from the STS and TRS are slightly higher. All four simulations produce an ice thickness 450 m too thin, with temperatures almost 4°C too high at the surface, mostly due to the lapse rate, and 11°C–12°C too high at the base.

4. Sensitivity Analysis

[58] Given the fact that the climate evolution that drives our GIS model is defined in an overly simplified way (see section 2.2), it is reasonable to assume a significant contribution of inadequacies in the past climate forcing to the misfit between the observed and modeled states of the present-day GIS (see section 3.2). Even in central Greenland, where surface temperature forcing is based on paleoclimate reconstruction, the precipitation history remains poorly constrained. In the following sections, we therefore aim at analyzing the sensitivity of the modeled ice thickness and basal thermal state of the present-day GIS to all major forcing components, namely precipitation, surface

Table 2. Modeled Versus Observed Basal Temperatures (°C) at the Deep Ice Core Sites of the GIS

	TRS	STS	MDS	U63S	Observed
GRIP	−2.64	−11.743	−3.711	−6.924	−8.56
GISP2	−2.672	−11.65	−3.581	−6.85	−9.05
NGRIP	−2.566[a]	−8.49	−2.62[a]	−2.612[a]	−2.4[a]
CC	−7.197	−13.13	−11.884	−8.57	−13
Dye 3	−1.337[a]	−1.339[a]	−1.5524	−2.26	−13.22
NEEM	−2.11[a]	−12.24	−6.6427	−4.99	Non-temperate[b]

[a]Temperate base.
[b]*Popp et al.* [2010] and *Dahl-Jensen* [2010].

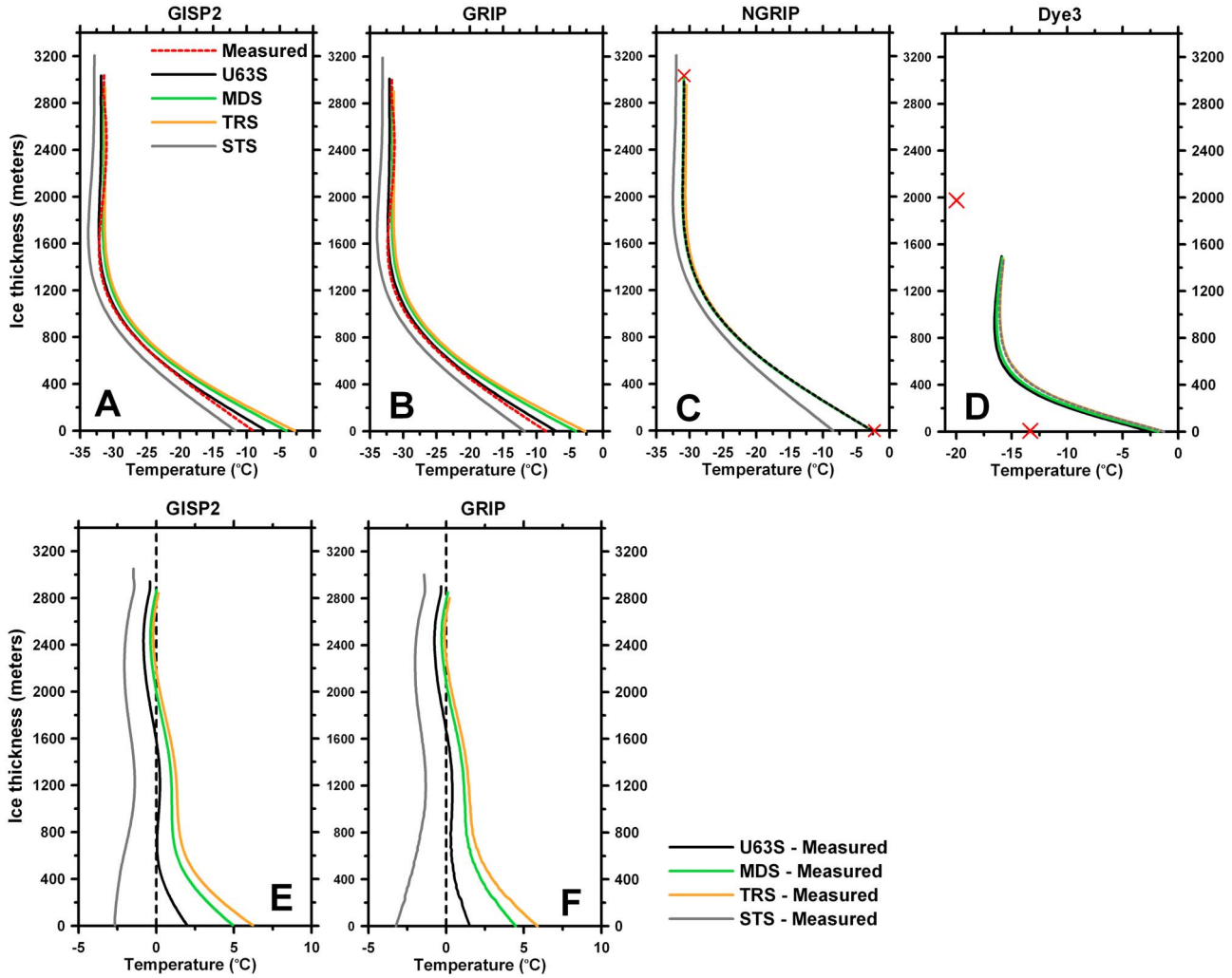

Figure 5. Simulated present-day temperature profiles resulting from the TRS (orange), STS (gray), MDS (green), and U63S (black) for the locations of (a) GISP2, (b) GRIP, (c) NGRIP and (d) Dye 3 ice cores (see Figure 1a). Differences between the measured and observed temperature profiles at the locations of the (e) GISP2 and (f) GRIP from the bedrock to the observed thickness of the ice surface. Dashed red curves indicate the measured temperatures at the GRIP and GISP2 sites. Red crosses indicate measured temperatures at the present-day base and ice surface.

temperature and GHF forcings, in order to estimate the potential of each forcing component to influence the agreement between the observations and the modeled quantities.

4.1. Sensitivity of the Modeled Basal Temperature and Thickness of the Present-Day GIS to Climate Forcing

[59] To analyze the possible effects of inadequacies in the past climate forcing on the ice thicknesses (Figure 3) and basal temperatures (Figure 4) of the present-day GIS, we designed four series of paleoclimatic simulations. These are driven by colder/warmer climate conditions and higher/lower precipitation rates during the last glacial (Wisconsin, 110 to 20 kyr BP) period and the Holocene period (11 kyr BP to the present) relative to the climate forcing employed by the reference simulation, U63S (details of each series of simulations are in Table 3). In the first two series of simulations, SS_TW and SS_TH, the temperature forcing is perturbed by increasing/decreasing surface temperature by a portion Pt (in %) of the surface temperature employed by the U63S for each grid point and time step during the Wisconsin and Holocene, respectively.

[60] Note that when we refer to a positive perturbation in surface temperature, for temperatures below 0°C, this will lead to a cooling of the climate forcing, and vice versa for a negative perturbation, e.g., a surface temperature of −40°C perturbed by +10% will be −44°C. This is expressed by

$$T_{ma}^{Pt}(\theta,\varphi,t) = T_{ma}(\theta,\varphi,t)\cdot\left(1+\frac{Pt}{100}\right),\ \text{for}\ T_{ma}<0. \qquad (19a)$$

[61] However, in some cases the mean annual surface temperature T_{ma} is positive. In these cases we still define

Table 3. Details of the Sensitivity Simulations

Series of Simulation[a]	Perturbed Forcing Component (units)	Perturbation Period (kyr BP)	Perturbation *Pt* (%) Relative to U63S[b]	Link Between *Pt* (%) and Pt_u (units)[c]	
				GRIP	Dye 3
SS_TW	Surface temperature, $T_{ma}(\theta, \varphi, t)$ (°C)	Wisconsin 110 – 20	−20, −15, −10, −5, +5, +10, +15, +20	+10% equals - 4.8°C	+10% equals -3.3 (°C)
SS_TH	Surface temperature, $T_{ma}(\theta, \varphi, t)$ (°C)	Holocene 11–0	−10, −5, +5, +10, +15, +20	+10% equals - 3.36°C	+10% equals - 2.36 (°C)
SS_PW	Precipitation, $P_{ma}(\theta, \varphi, t)$ (mm/a)	Wisconsin 110–20	−20, −15, −10, −5, +5, +10, +15, +20	+10% equals + 12.3 mm/a	+10% equals + 28.1 (mm/a)
SS_PH	Precipitation, $P_{ma}(\theta, \varphi, t)$ (mm/a)	Holocene 11–0	−20, −15, −10, −5, +5, +10, +15, +20	+10% equals + 20.9 mm/a	+10% equals + 52.7 (mm/a)
SS_GHF	GHF (mW/m^2)	250–0	−20, −15, −10, −5, +5, +10, +15, +20	10% = 6.3 (mW/m^2)	

[a]SS, sensitivity simulations; T, temperature; P, precipitation; W, Wisconsin; H, Holocene; GHF, geothermal heat flux.
[b]Negative perturbation in surface temperature, *Pt*, corresponds to warmer climate conditions and vice versa.
[c]Pt_u is the deviation of perturbed forcing component from the unperturbed one (as in the U63S) averaged over the perturbation time at the GRIP/Dye 3 location.

a positive perturbation as a cooling of the climate forcing, and vice versa for a negative perturbation, e.g., a surface temperature of +5°C perturbed by +10% becomes +4.5°C. This is in turn expressed as

$$T_{ma}^{Pt}(\theta, \varphi, t) = T_{ma}(\theta, \varphi, t) \cdot \left(1 - \frac{Pt}{100}\right), \text{ for } T_{ma} > 0. \qquad (19b)$$

[62] In the second two series of simulations, SS_PW and SS_PH, we perturb precipitation forcing by a portion *Pt* (in %) of the precipitation rates employed by the U63S, again for each grid point and time step and during the same perturbation periods:

$$P_{ma}^{Pt}(\theta, \varphi, t) = P_{ma}(\theta, \varphi, t) \cdot \left(1 + \frac{Pt}{100}\right), \qquad (20)$$

where a positive perturbation *Pt* leads to increased precipitation, and the opposite for a negative perturbation.

[63] The resulting present-day basal temperatures and ice thicknesses as functions of the perturbations in precipitation (left) and surface temperature (middle) forcings during the Wisconsin (blue) and Holocene (red) at the locations of the GRIP (crosses) and Dye3 (diamonds) drill sites are shown in Figures 6a–6f.

[64] At the GRIP site, the responses of basal temperature and ice thickness to perturbations in precipitation forcing are nearly linear, as opposed to their responses to perturbations in the surface temperature forcing. Nonlinearity in the response of the GRIP ice column to increasing Wisconsin temperature is due to the changing rheological properties of ice as it approaches the pressure-melting point, while the nonlinear response to even moderately warmer Holocene climate (relative to the U63S forcing) is caused by instabilities in the GIS. This is indicated by the GRIP ice column being 400 m thinner under conditions of a 10% warmer Holocene climate (Figure 6f) and by the complete disintegration of the southern GIS as a result of the 5% higher temperatures during the Holocene (Figure 6d).

[65] Both the southern and central GIS areas appear to be very sensitive to perturbations in Holocene precipitation. A 10%-deficit of precipitation (relative to the U63S forcing) results in the ice sheet being 250 m thinner at Dye 3 and 65 m thinner at GRIP, while a 10% higher Holocene precipitation results in 65 to 70 m thicker ice in both locations (Figures 6a and 6c). The latter responses of the present-day GIS indicate that the scenarios for the Holocene climate being warmer or drier than that employed by the U63S are unlikely to be realistic.

[66] The effects of the Wisconsin precipitation forcing on the GRIP thickness are rather minor (Figure 6c, 18 m per 10%), whereas the present-day Summit grows extensively in response to perturbations in the Wisconsin temperature forcing (Figure 6f). Thus, a 10% cooling of the Wisconsin climate conditions leads to almost 100 m thicker ice. The present-day basal temperature is strongly affected by the Wisconsin precipitation (0.55°C per 10%) and surface temperature (2°C per 10%) forcings, whereas the effects of the Holocene forcing components on basal temperatures are less pronounced (0.17°C and 0.04°C per 10%, respectively).

[67] At Dye 3 location, the present-day ice thickness responds strongly to the perturbations in the Holocene climate conditions, while remaining rather insensitive to changes in both the Wisconsin precipitation and temperature forcings (Figure 6a and 6d). By contrast, the responses of the Dye 3 basal thermal conditions to perturbations in Holocene and Wisconsin temperatures are very similar (Figure 6e), with basal temperature decreasing by approximately 0.25°C for each 10% that the surface temperature is decreased. Perturbations in the Holocene and Wisconsin precipitation forcings have the opposite effects on basal temperatures, showing that an increase in Holocene precipitation makes the southern GIS thicker, but also increases basal temperatures, thereby enhancing the misfit between the measured and modeled basal temperatures.

4.2. Relative Effects of the Climate and GHF Forcing Components on the Present-Day GIS

[68] The second part of the sensitivity analysis aims to examine the relative effects of the three major forcings of the GIS model, namely the precipitation and temperature histories and the GHF forcing, on the basal thermal state and ice thickness of the present-day GIS. For this purpose, we introduce a fifth series of paleoclimatic simulations

(SS_GHF), which is driven by a number of spatially uniform GHF forcings. SS_GHF uses GHF values that are up to 20% lower or higher than the value of 63 mW/m^2 employed by the reference simulation (Table 3). The resulting present-day basal temperatures and ice thicknesses as functions of perturbations in GHF at the locations of the GRIP (crosses) and Dye3 (diamonds) drill sites are shown in Figures 6g–6i.

[69] The GHF forcing strongly affects the modeled present-day GRIP thickness (Figure 6i), while its effects on the Dye 3 ice thickness are rather moderate (Figure 6g), especially in comparison to the effects of the Holocene climate

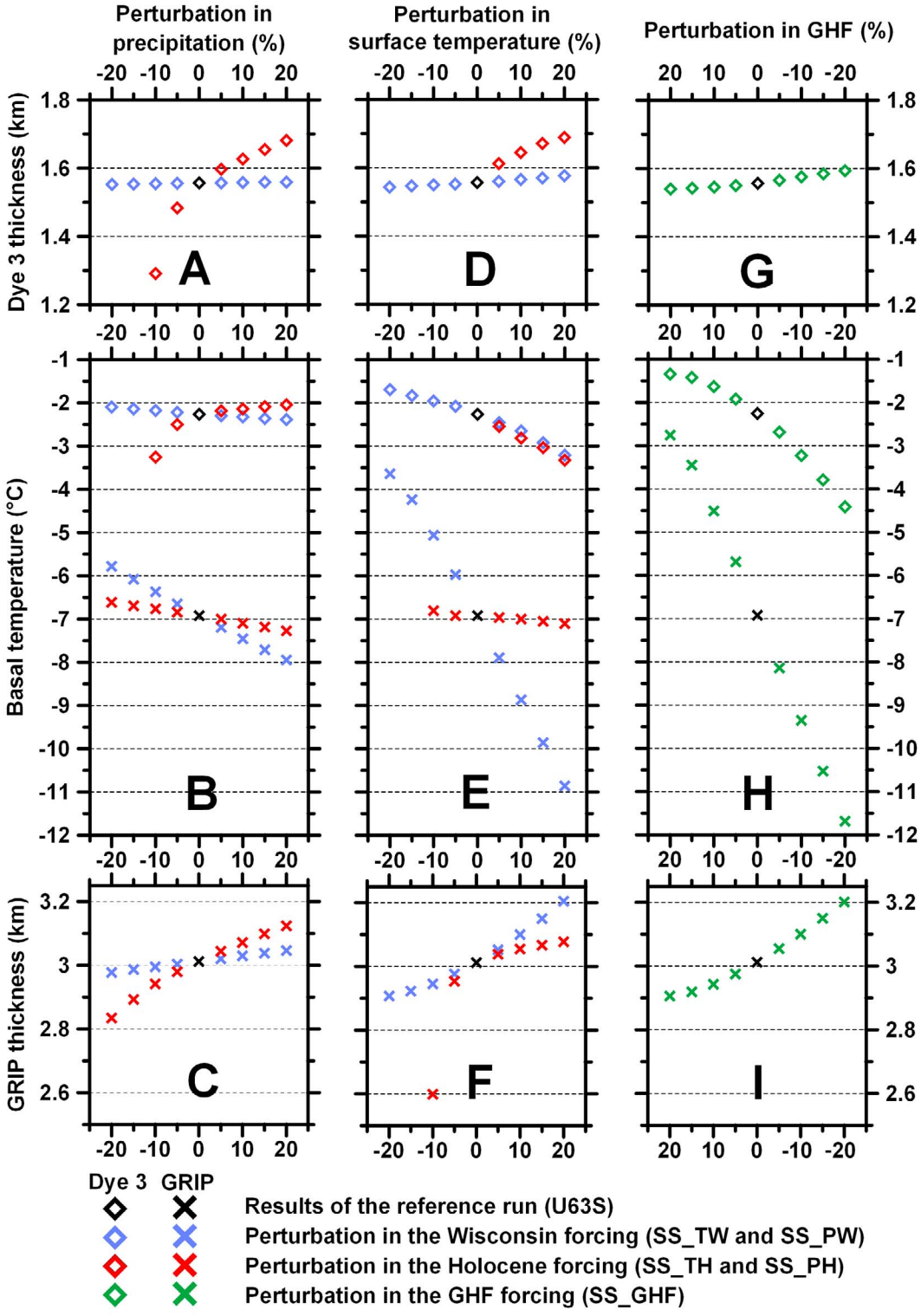

Figure 6

forcing (Figures 6a and 6d). In general, the responses of both basal temperatures and ice thicknesses to the same perturbations in the GHF forcing are stronger at the GRIP site (2.45°C and 100 m per 10%, respectively) than at Dye 3 (1.1°C and 20 m per 10%, respectively). It is also striking how similar the responses of the GRIP and Dye 3 ice thicknesses are to the perturbations in the GHF and Wisconsin temperature forcings. However, in both locations, the responses of basal temperatures to the changes in the GHF forcing are considerably stronger than their responses to the Wisconsin temperature perturbations.

[70] Since the response of the GRIP basal thermal state to all forcing components is almost linear, we can link the effects of the GHF forcing and the two climate forcing components by comparing their contributions. Even in those cases where the responses are nonlinear, we are still able to provide estimates for the relative contributions of the different forcing components. We will only consider climate forcings during those perturbation periods which significantly influence the basal thermal state, namely Wisconsin precipitation and temperature at the GRIP location and both the Wisconsin and Holocene climate forcings at Dye 3.

[71] The effect of a perturbation in the uniform GHF forcing by 10% (6.3 mW/m^2) is equivalent to those from the perturbations in the Wisconsin temperature forcing by 12.5% at the GRIP location and by approximately 20% at the Dye 3 site. The response of basal temperatures to the maximum perturbation in Wisconsin precipitation (20%) resembles their responses to a GHF perturbation of 3 to 5% (2–3.1 mW/m^2) in both the central and southern GIS areas. A 20%-perturbation in Holocene temperature contributes to the Dye 3 basal thermal regime as much as an 11%-perturbation in the GHF forcing (7 mW/m^2), while the effects of Holocene precipitation on the southern GIS appear quite different from the effects of perturbing the GHF forcing.

5. Discussion

5.1. Spatially Variable GHF Models Versus Spatially Uniform GHF Distribution Under the GIS

[72] The results presented in section 3.2 suggest that the simulation U63S, driven by a spatially uniform GHF forcing, produces a considerably better fit to the majority of the observational data considered in this study than the other simulations, driven by spatially variable GHF forcings. This raises questions about the credibility of these GHF models within the context of GIS modeling.

[73] The GHF value of 63 mW/m^2 used in the U63S represents the mean of the averaged GHF values over the Greenland territory that are suggested by the magnetic (68 mW/m^2) and seismic (58 mW/m^2) GHF models. The tectonic GHF model was not considered while calculating this mean value, because a number of previous studies have already identified the tectonic GHF model as providing too high GHFs under most of the GIS-covered territory [e.g., *Greve*, 2005; *Tarasov and Peltier*, 2003]. This conclusion is well supported by the results of the present study (see section 3.2). In any case, the GHF value of 63 mW/m^2 is significantly larger than those used by most GIS modeling studies [e.g., *Abe-Ouchi et al.*, 1994; *Calov and Hutter*, 1996; *Huybrechts*, 2002], but is supported by the results of *Greve* [2000] and *Lhomme et al.* [2005].

[74] Despite the value of 63 mW/m^2 lying between the two averages of the seismic and magnetic models, the U63S reveals a close correspondence to the results of the MDS, but not to the STS (Figures 2 and 3). This fact can be explained by the following effects: (1) Both the magnetic and spatially uniform GHF models include GHF values that are sufficiently high to form large areas with basal temperatures close to the pressure-melting point. (2) The magnetic model gives a mosaic of small-scale patterns with higher and lower GHF values that do not have the power to strongly heat or cool large parts of the GIS. (3) By contrast, the low GHFs provided by the seismic model enhance the thickening of the most ancient central and northern parts of the GIS throughout the modeled history.

[75] In the northern, western and southern-southeastern parts of Greenland, both the magnetic and seismic models reveal a close correspondence, suggesting similar GHF features and a northwest to southeast horizontal gradient. Thus, a large difference between the averaged GHF values for these two models (10 mW/m^2) is mostly due to an 8-to-35-mW/m^2 difference between the GHF values predicted by the two models in central Greenland (see Figures 1b and 1c). The results discussed in section 3.2 indicate that the STS produces systematically too low basal temperatures in the central GIS as opposed to the MDS, which produces too-high basal temperature values in the central non-temperate areas where observations exist (see Table 2). The mean GHF value of 63 mW/m^2 lies between the too-low GHF values from the seismic model and too-high GHF values from the magnetic model, thereby producing a better fit with the temperature measurements in central Greenland. This fact indicates that both the seismic and magnetic GHF models produce reasonable GHF values for the Greenland

Figure 6. Simulated basal temperatures and ice thicknesses resulting from the series of sensitivity tests, SS_TW and SS_PW (blue), SS_TH and SS_PH (red), SS_GHF (green), and the reference simulation, U63S (black), at the locations of the GRIP (crosses) and Dye 3 (diamonds) boreholes. The responses of modeled ice thicknesses to perturbations in the Wisconsin (blue) and Holocene (red) precipitation rates are shown at the locations of (a) Dye 3 and (c) GRIP. (b) Corresponding responses of modelled basal temperatures at Dye 3 (diamonds) and GRIP (crosses) are given. The responses of modeled ice thicknesses to perturbations in the Wisconsin and Holocene surface temperature forcing are shown at the locations of (d) Dye 3 and (f) GRIP. (e) Corresponding responses of modelled basal temperatures at Dye 3 (diamonds) and GRIP (crosses) are given. Finally, the responses of modeled ice thicknesses to perturbations in the GHF forcing are shown at the locations of (g) Dye 3 and (i) GRIP. (h) Corresponding responses of modelled basal temperatures at both locations are given. The measured basal temperatures at these two boreholes are given in Table 2. The observed ice thicknesses are 3.028 km at GRIP and 2.035 km at Dye 3.

region, but are unlikely to correctly represent the actual spatial patterns of the GHF distribution.

5.2. Possible Reasons for the Model's Failure in Southern Greenland

[76] In southern Greenland, all four simulations failed to reproduce either the observed ice topography (Figure 3) or the measured cold basal conditions (Figures 4 and 5), giving basal temperatures that are 11°C too high at the location of the Dye 3 drill site, and ice that is 400 to 600 m too thin. In this region, where we have the largest misfit with observations, all GHF models provide relatively high GHFs between 58 and 82 mW/m^2 (tectonic model: 72 to 82 mW/m^2, seismic model: 70 to 80 mW/m^2, magnetic model: 58 to 75 mW/m^2, and spatially uniform model: 63 mW/m^2). Such high GHF values contradict the findings of previous studies that suggest low GHFs (20 to 45 mW/m^2) in this region [*Dahl-Jensen et al.*, 1998; *Huybrechts*, 1996; *Greve*, 2005; *Gundestrup and Hansen*, 1984; *Lhomme et al.*, 2005; *Tarasov and Peltier*, 2003]. The results of the above mentioned studies are also supported by information about low GHF values obtained from the southern boreholes, Ivigtut and Ilimaussaq [*Sass et al.*, 1972]. That is why the U63S and MDS, which are defined by slightly lower GHF values in southern Greenland, show better agreement with the observed basal conditions at the Dye 3 site compared to the other two simulations, STS and TRS.

[77] As discussed above, the tectonic model suffers from generally too-high GHF values under most of the GIS, including the southern ice-covered region. In addition, the resolution of this GHF model is too crude (over 1000 km) to capture the spatial variations in GHF in this region, which is 500 km wide and 700 km long. It has been suggested by *Fox Maule et al.* [2009] that in southern Greenland, the too-high GHF values provided by the magnetic GHF model may be due to an overestimation of the crustal heat production. Inaccuracies in the modeled crustal heat production are likely to be significant in the south of Greenland, where measurements obtained from the fairly close boreholes, Ivigtut and Ilimaussaq [*Sass et al.*, 1972], reveal strong spatial variability in surface heat production. Given the fact that the seismic and magnetic models are based on somewhat similar assumptions about crustal heat production [*Fox Maule et al.*, 2009], it is not surprising that both models overestimate GHF values in this region. Thus, the large discrepancies between the observed and modeled basal temperatures and ice thicknesses at the Dye 3 station may be partly attributed to inaccuracies in the GHF forcing at this location.

[78] The sensitivity analysis presented in sections 4.1 and 4.2 suggests that the underestimated ice thickness in southern Greenland is possibly due to the uncertainties in the Holocene climate conditions rather than the GHF forcing (Figures 6a, 6d and 6g). The effects of the Holocene precipitation forcing are such that, while improving an agreement with one observable (ice thickness or basal temperature), they increase the disagreement with another (see section 4.1). Thus, the misfit between the observed and modeled ice topographies is unlikely to be due to strongly underestimated Holocene precipitation (Figure 3). It is therefore clear that a large portion of the misfit between the observed and modeled southern GIS can be amended by decreasing the GHF to the lower values suggested by the previous studies (i.e., 20–45 mW/m^2) and improving the regional surface temperature forcing, especially for the Holocene period, by using the surface temperature reconstruction inferred from the Dye 3 ice core [*Dahl-Jensen et al.*, 1998].

[79] Finally, we expect that another significant contribution to the misfit between the observed and modeled southern GIS is due to the simplifying assumptions within the modeling approach used [e.g., *Souček and Martinec*, 2008], in particular the absence of explicit ice stream dynamics [*Pattyn*, 2010].

5.3. Uncertainties in Past Climate Forcing and Their Effects on the Present-Day Summit of the GIS

[80] The sensitivity analysis presented in section 4 demonstrates that the effects of different forcing components on the GIS are location dependent, therefore the conclusions based on the analysis of the two locations, both of which are in close proximity to the GIS divide, are not easy to extend to the GIS as a whole. Our results are in agreement with those from previous studies, in that for thinner or more dynamic ice sheet areas, the roles of both the GHF and the glacial climate diminish. However, even in the relatively thin and dynamic southern GIS, which is fostered by the highest precipitation rates across Greenland, basal conditions are still strongly affected by the glacial climate forcing (Figure 6e).

[81] The results of the sensitivity analysis suggest that the misfit between the observed and modeled basal temperatures in the central GIS could, to some extent, be explained by inadequacies in the Wisconsin forcing. Given the fact that, in the Summit region, the modeled ice thickness is close to the observed one and the surface temperature history is relatively well constrained, it is the inadequacies in the Wisconsin precipitation forcing that should influence the values of the modeled basal temperatures to a greater extent. By contrast, the deviations of the modeled vertical temperature gradients from the observed ones are believed to be mainly a product of inaccurate GHF forcing and simplifying assumptions about ice rheology and internal energy evolution within the employed dynamic ice sheet model.

6. Conclusions

[82] We have designed a series of paleoclimatic simulations and sensitivity experiments that have allowed us to assess the effects of three GHF forcings, namely the magnetic model of *Fox Maule et al.* [2009], the seismic model of *Shapiro and Ritzwoller* [2004], and the tectonic model of *Pollack et al.* [1993], on the present-day GIS within the context of dynamic ice sheet modeling. Due to the large differences in the regional GHF patterns and overall heat flux into the GIS body predicted by the GHF models, the three paleoclimatic simulations suggest quite dissimilar scenarios for the history of the GIS, resulting in large differences in its present-day thermal regime and topography. After comparing the direct temperature measurements inferred from the deep ice core sites and the observed GIS thickness with the equivalent modeled quantities, we conclude that the simulation controlled by the tectonic GHF model gives a present-day ice sheet that is largely too warm and too thin. This confirms findings of previous studies indicating that the tectonic GHF model generally overestimates GHF values under most of the ice-covered Greenland region [*Greve*, 2005;

Tarasov and Peltier, 2003]. On the other hand, the simulation controlled by the seismic GHF model produces an ice sheet that is too cold, and 200 m too thick, over central and northern Greenland, whereas the resulting southern GIS is 200 to 600 m too thin and too warm by 11°C degrees at the base. The third simulation, using the magnetic GHF forcing, exhibits a good agreement with respect to the observed state of the northern GIS, but results in too-high temperatures in the Summit region and again fails to reproduce either the surface topography or the observed low basal temperatures in southern Greenland. Finally, for the purpose of comparison, we have designed a fourth simulation driven by a spatially uniform GHF forcing under the entire GIS, with a constant GHF value of 63 mW/m^2 (this being a mean of the averaged GHF values from the magnetic and seismic models). This simulation provides a considerably better fit with the majority of the used observational data and raises questions about the credibility of the three addressed GHF models within the framework of GIS modeling studies.

[83] Sensitivity experiments suggest that the misfit between the modeled and measured basal temperatures in central Greenland arises, to a large part, from inaccurate GHF and Wisconsin precipitation forcings, whereas the misfit between the measured and modeled vertical temperature gradients is mostly due to GHF forcing and simplifications within the modeling approach.

[84] These sensitivity experiments also reveal that the failures of all simulations in the southern part of the GIS can be attributed to both the overestimated GHF values in this region and inaccuracies in the past surface temperature forcing, in particular during the Holocene period. The results of previous studies [*Dahl-Jensen et al.*, 1998; *Huybrechts*, 1996; *Greve*, 2005; *Gundestrup and Hansen*, 1984; *Tarasov and Peltier*, 2003] suggest that GHF values should be two to three times smaller than the values proposed by the addressed GHF models in southern Greenland. Although a significant decrease in Wisconsin and Holocene surface temperatures could possibly result in colder present-day basal conditions in this region, the temperature forcing required to fit the observed basal temperatures is unrealistically cold and not supported by past climate reconstructions.

[85] **Acknowledgments.** This study is a part of the IceGeoHeat initiative (I. Rogozhina, A. Petrunin, I. Artemieva, M. K. Kaban, B. Steinberger, A. P. M. Vaughan, I. Kukkonen, A. Shulgin, I. Koulakov, Z. Martinec, W. Stolk). We are thankful to three anonymous reviewers, Alan P. M. Vaughan, James Fastook and two editors for their helpful remarks that have improved the paper considerably. Special thanks to Cathrine Fox Maule and Lev Tarasov for sharing their GHF models with us. Zdenek Martinec acknowledges the support from the Grant Agency of the Czech Republic through grant 205/09/0546. Ralf Greve was supported by a Grant-in-Aid for Scientific Research A (22244058) from the Japan Society for the Promotion of Science (JSPS).

References

Abe-Ouchi, A., H. Blatter, and A. Ohmura (1994), How does the Greenland ice sheet geometry remember the ice age?, *Global Planet. Change*, *9*, 133–142, doi:10.1016/0921-8181(94)90012-4.

Alley, R. B., et al. (1993), Abrupt increase in Greenland snow accumulation at the end of the Younger Dryas event, *Nature*, *362*, 527–529, doi:10.1038/362527a0.

Anderson, K. K., et al. (2004), High-resolution record of Northern Hemisphere climate extending into the last interglacial period, *Nature*, *431*(7005), 147–151, doi:10.1038/nature02805.

Augustin, L., et al. (2004), Eight glacial cycles from an Antarctic ice core, *Nature*, *429*, 623–628, doi:10.1038/nature02599.

Bamber, J. L., R. L. Layberry, and S. P. Gogineni (2001), A new ice thickness and bed data set for the Greenland ice sheet: 1. Measurement, data reduction, and errors, *J. Geophys. Res.*, *106*(D24), 33,773–33,780.

Barbante, C., et al. (2006), One-to-one coupling of glacial climate variability in Greenland and Antarctica, *Nature*, *444*, 195–198, doi:10.1038/nature05301.

Bell, R. E. (2008), The role of subglacial water in ice-sheet mass balance, *Nat. Geosci.*, *1*, 297–304, doi:10.1038/ngeo186.

Brinkerhoff, D. J., T. W. Meierbachtol, J. V. Johnson, and J. T. Harper (2011), Sensitivity of the frozen/melted basal boundary to perturbations of basal traction and geothermal heat flux: Isunnguata Sermia, western Greenland, *Ann. Glaciol.*, *52*(59), 43–50, doi:10.3189/172756411799096330.

Buchardt, S. L., and D. Dahl-Jensen (2007), Estimating the basal melt rate at NorthGRIP using a Monte Carlo technique, *Ann. Glaciol.*, *45*, 137–142, doi:10.3189/172756407782282435.

Bueler, E., C. S. Lingle, J. A. Kallen-Brown, D. N. Covey, and L. N. Bowman (2005), Exact solutions and verification of numerical models for isothermal ice sheets, *J. Glaciol.*, *51*, 291–306, doi:10.3189/172756505781829449.

Calanca, P., H. Gilgen, S. Ekholm, and A. Ohmura (2000), Gridded temperature and accumulation distributions for use in cryospheric models, *Ann. Glaciol.*, *31*, 118–120, doi:10.3189/172756400781820345.

Calov, R., and R. Greve (2005), A semi-analytical solution for the positive degree-day model with stochastic temperature variations, *J. Glaciol.*, *51*(172), 173–175.

Calov, R., and K. Hutter (1996), The thermomechanical response of the Greenland ice sheet to various climate scenarios, *Clim. Dyn.*, *12*, 243–260, doi:10.1007/BF00219499.

Chandler, D. M., A. L. Hubbard, B. P. Hubbard, and P. W. Nienow (2006), A Monte Carlo error analysis for basal sliding velocity calculations, *J. Geophys. Res.*, *111*, F04005, doi:10.1029/2006JF000476.

Clow, G. D., R. W. Saltus, and E. D. Waddington (1996), A new high-precision borehole-temperature logging system used at GISP2, Greenland, and Taylor Dome, Antarctica, *J. Glaciol.*, *42*, 576–584.

Cuffey, K. M., G. D. Clow, R. B. Alley, M. Stuiver, E. D. Waddington, and R. W. Saltus (1995), Large Arctic temperature-change at the Wisconsin-Holocene glacial transition, *Science*, *270*, 455–458, doi:10.1126/science.270.5235.455.

Dahl-Jensen, D. (2010), The Eemian ice from the new Greenland ice core at NEEM, Abstract C24A-06 presented at 2010 Fall Meeting, AGU, San Francisco, Calif., 13–17 Dec.

Dahl-Jensen, D., K. Mosegaard, N. Gundestrup, G. D. Clow, S. J. Johnsen, A. W. Hansen, and N. Balling (1998), Past temperatures directly from the Greenland ice sheet, *Science*, *282*, 268–271, doi:10.1126/science.282.5387.268.

Dahl-Jensen, D., N. Gundestrup, P. Gogineni, and H. Miller (2003), Basal melt at NorthGRIP modeled from borehole, ice-core and radio-echo sounder observations, *Ann. Glaciol.*, *37*, 207–212, doi:10.3189/172756403781815492.

Dansgaard, W., et al. (1993), Evidence for general instability of past climate from a 250-kyr ice-core record, *Nature*, *364*(6434), 218–220, doi:10.1038/364218a0.

Fahnestock, M., W. Abdalati, I. Joughin, J. Brozena, and P. Gogineni (2001), High geothermal heat flow, basal melt, and the origin of rapid ice flow in central Greenland, *Science*, *294*, 2338–2342, doi:10.1126/science.1065370.

Fox Maule, C., M. E. Purucker, N. Olsen, and K. Mosegaard (2005), Heat flux in Antarctica revealed from satellite magnetic data, *Science*, *309*, 464–467, doi:10.1126/science.1106888.

Fox Maule, C., M. E. Purucker, and N. Olsen (2009), Inferring magnetic crustal thickness and geothermal heat flux from crustal magnetic field models, *Rep. 09-09*, Danish Meteorol. Inst., Copenhagen. [available at http://www.dmi.dk/dmi/dkc09-09.pdf.]

Goldberg, D. N., and O. V. Sergienko (2011), Data assimilation using a hybrid ice flow model, *Cryosphere*, *5*, 315–327, doi:10.5194/tc-5-315-2011.

Greenland Ice Core Project members (1993), Climate instability during the last interglacial period recorded in the GRIP ice core, *Nature*, *364*, 203–207, doi:10.1038/364203a0.

Greve, R. (1995), Thermomechanisches Verhalten polythermer Eisschilde - Theorie, Analytik, Numerik, PhD thesis, Dep. of Mech., Darmstadt Univ. of Technol., Darmstadt, Germany.

Greve, R. (1997a), A continuum-mechanical formulation for shallow polythermal ice sheets, *Philos. Trans. R. Soc. London A*, *355*(1726), 921–974.

Greve, R. (1997b), Application of a polythermal three-dimensional ice sheet model to the Greenland ice sheet: Response to steady-state and transient climate scenarios, *J. Clim.*, *10*(5), 901–918, doi:10.1175/1520-0442(1997)010<0901:AOAPTD>2.0.CO;2.

Greve, R. (2000), On the response of the Greenland ice sheet to greenhouse climate change, *Clim. Change*, *46*(3), 289–303, doi:10.1023/A:1005647226590.

Greve, R. (2001), Glacial isostasy: Models for the response of the Earth to varying ice loads, in *Continuum Mechanics and Applications in Geophysics and the Environment*, edited by B. Straughan et al., pp. 307–325, Springer, Berlin.

Greve, R. (2005), Relation of measured basal temperatures and the spatial distribution of the geothermal heat flux for the Greenland ice sheet, *Ann. Glaciol.*, *42*, 424–432, doi:10.3189/172756405781812510.

Greve, R., and H. Blatter (2009), *Dynamics of Ice Sheets and Glaciers*, Springer, Berlin, doi:10.1007/978-3-642-03415-2.

Greve, R., M. Weis, and K. Hutter (1998), Palaeoclimatic evolution and present conditions of the Greenland ice sheet in the vicinity of Summit: An approach by large-scale modeling, *Paleoclimates*, *2*(2–3), 133–161.

Grinsted, A., and D. Dahl-Jensen (2002), A Monte Carlo-tuned model of the flow in the NorthGRIP area, *Ann. Glaciol.*, *35*, 527–530, doi:10.3189/172756402781817130.

Gudmundsson, G. H., and M. Raymond (2008), On the limit to resolution and information on basal properties obtainable from surface data on ice streams, *Cryosphere*, *2*(2), 167–178, doi:10.5194/tc-2-167-2008.

Gundestrup, N. S., and B. L. Hansen (1984), Bore-hole survey at Dye 3, South Greenland, *J. Glaciol.*, *30*, 282–288.

Hewitt, C. D., and J. F. B. Mitchell (1997), Radiative forcing and response of a GCM to ice age boundary conditions: Cloud feedback, and climate sensitivity, *Clim. Dyn.*, *13*(11), 821–834, doi:10.1007/s003820050199.

Hindmarsh, R. C. A., and E. Le Meur (2001), Dynamical processes involved in the retreat of marine ice sheets, *J. Glaciol.*, *47*(157), 271–282, doi:10.3189/172756501781832269.

Hutter, K. (1982), A mathematical model of polythermal glaciers and ice sheets, *Geophys. Astrophys. Fluid Dyn.*, *21*, 201–224, doi:10.1080/03091928208209013.

Hutter, K. (1983), *Theoretical Glaciology: Material Science of Ice and the Mechanics of Glaciers and Ice Sheets*, D. Reidel, Dordrecht, Netherlands.

Huybrechts, P. (1996), Basal temperature conditions of the Greenland ice sheet during the glacial cycles, *Ann. Glaciol.*, *23*, 226–236.

Huybrechts, P. (2002), Sea-level changes at the LGM from icedynamic reconstructions of the Greenland and Antarctic ice sheets during the glacial cycles, *Quat. Sci. Rev.*, *21*(1–3), 203–231, doi:10.1016/S0277-3791(01)00082-8.

Huybrechts, P., and J. de Wolde (1999), The dynamic response of the Greenland and Antarctic ice sheets to multiple-century climatic warming, *J. Clim.*, *12*(8), 2169–2188, doi:10.1175/1520-0442(1999)012<2169:TDROTG>2.0.CO;2.

Johnsen, S. J., D. Dahl-Jensen, W. Dansgaard, and N. S. Gundestrup (1995), Greenland paleotemperatures derived from GRIP borehole temperature and ice core isotope profiles, *Tellus, Ser. B*, *47*(5), 624–629.

Johnsen, S. J., D. Dahl-Jensen, N. Gundestrup, J. P. Steffensen, H. B. Clausen, H. Miller, V. Masson-Delmotte, A. E. Sveinbjörnsdottir, and J. White (2001), Oxygen isotope and palaeotemperature records from six Greenland ice-core stations: Camp Century, Dye-3, GRIP, GISP2, Renland and NorthGRIP, *J. Quat. Sci.*, *16*, 299–307, doi:10.1002/jqs.622.

Johnson, J., and J. L. Fastook (2002), Northern Hemisphere glaciation and its sensitivity to basal melt water, *Quat. Int.*, *95–96*, 65–74, doi:10.1016/S1040-6182(02)00028-9.

Jouzel, J., et al. (1993), Extending the Vostok ice-core record of paleoclimate to the penultimate glacial period, *Nature*, *364*, 407–412, doi:10.1038/364407a0.

Jouzel, J., et al. (1997), Validity of the temperature reconstruction from water isotopes in ice cores, *J. Geophys. Res.*, *102*, 26,471–26,487, doi:10.1029/97JC01283.

Layberry, R. L., and J. L. Bamber (2001), A new ice thickness and bed data set for the Greenland ice sheet 2. Relationship between dynamics and basal topography, *J. Geophys. Res.*, *106*(D24), 33,781–33,788, doi:10.1029/2001JD900053.

Le Meur, E., and P. Huybrechts (1996), A comparison of different ways of dealing with isostasy: Examples from modelling the Antarctic ice sheet during the last glacial cycle, *Ann. Glaciol.*, *23*, 309–317.

Lhomme, N., G. K. C. Clarke, and S. J. Marshall (2005), Tracer transport in the Greenland Ice Sheet: Constraints on ice cores and glacial history, *Quat. Sci. Rev.*, *24*, 173–194, doi:10.1016/j.quascirev.2004.08.020.

Llubes, M., C. Lanseau, and F. Remy (2006), Relations between basal condition, subglacial hydrological networks and geothermal flux in Antarctica, *Earth Planet. Sci. Lett.*, *241*, 655–662, doi:10.1016/j.epsl.2005.10.040.

Marsiat, I. (1994), Simulation of the Northern Hemisphere continental ice sheets over the last glacial–interglacial cycle: Experiments with a latitude–longitude vertically integrated ice sheet model coupled to a zonally averaged climate model, *Palaeoclimates*, *1*(1), 59–98.

Maxwell, D., M. Truffer, S. Avdonin, and M. Stuefer (2008), An iterative scheme for determining glacier velocities and stresses, *Ann. Glaciol.*, *36*, 197–204.

Meese, D., R. Alley, T. Gow, P. M. Grootes, P. Mayewski, M. Ram, K. Taylor, E. Waddington, and G. Zielinski (1994), Preliminary depth-age scale of the GISP2 ice core, *Spec. Rep. 94–1*, U.S. Army Corps of Eng., Cold Reg. Res. and Eng. Lab, Hanover, N. H.

Morland, L. W. (1984), Thermomechanical balances of ice sheet flows, *Geophys. Astrophys. Fluid Dyn.*, *29*, 237–266, doi:10.1080/03091928408248191.

Paterson, W. S. B. (1994), *The Physics of Glaciers*, 3rd ed., Elsevier, Oxford, U. K.

Pattyn, F. (2010), Antarctic subglacial conditions inferred from a hybrid ice sheet/ice stream model, *Earth Planet. Sci. Lett.*, *295*, 451–461, doi:10.1016/j.epsl.2010.04.025.

Petit, J. R., et al. (1999), Climate and atmospheric history of the past 420,000 years from the Vostok ice core, Antarctica, *Nature*, *399*(6735), 429–436, doi:10.1038/20859.

Pollack, H. N., S. J. Hurter, and J. R. Johnson (1993), Heat flow from the Earth's interior: Analysis of the global data set, *Rev. Geophys.*, *31*, 267–280, doi:10.1029/93RG01249.

Pollard, D., R. M. DeConto, and A. A. Nyblade (2005), Sensitivity of Cenozoic Antarctic ice sheet variations to geothermal heat flux, *Global Planet. Change*, *49*, 63–74, doi:10.1016/j.gloplacha.2005.05.003.

Popp, T. J., D. Dahl-Jensen, S. J. Johnsen, and J. Steffensen, and the Neem Isotope Consortium (2010), The North Greenland Eemian (NEEM) ice drilling: Isotopic profiles, regional climate gradients, and abrupt climate change, Abstract C23D-07, presented at 2010 Fall Meeting, AGU, San Francisco, Calif., 13–17 Dec.

Reeh, N. (1991), Parameterization of melt rate and surface temperature on the Greenland ice sheet, *Polarforschung*, *59*(3), 113–128.

Ritz, C. (1987), Time dependent boundary conditions for calculation of temperature fields in ice sheets, *IAHS Publ.*, *170*, 207–216.

Ritz, C., A. Fabre, and A. Letreguilly (1996), Sensitivity of a Greenland ice sheet model to ice flow and ablation parameters: Consequences for the evolution through the last climatic cycle, *Clim. Dyn.*, *13*(1), 11–23, doi:10.1007/s003820050149.

Rogozhina, I., Z. Martinec, J. M. Hagedoorn, M. Thomas, and K. Fleming (2011), On the long-term memory of the Greenland Ice Sheet, *J. Geophys. Res.*, *116*, F01011, doi:10.1029/2010JF001787.

Sass, J. H., B. L. Nielsen, H. A. Wollenberg, and R. J. Munroe (1972), Heat flow and surface radioactivity at two sites in South Greenland, *J. Geophys. Res.*, *77*, 6435–6444, doi:10.1029/JB077i032p06435.

Shapiro, N. M., and M. H. Ritzwoller (2002), Monte-Carlo inversion for a global shear velocity model of the crust and upper mantle, *Geophys. J. Int.*, *151*, 88–105, doi:10.1046/j.1365-246X.2002.01742.x.

Shapiro, N. M., and M. H. Ritzwoller (2004), Inferring surface heat flux distributions guided by a global seismic model: Particular application to Antarctica, *Earth Planet. Sci. Lett.*, *223*, 213–224, doi:10.1016/j.epsl.2004.04.011.

Smith, B. E., H. A. Fricker, I. R. Joughin, and S. Tulaczyk (2009), An inventory of active subglacial lakes in Antarctica detected by ICESat (2003–2008), *J. Glaciol.*, *55*(192), 573–595, doi:10.3189/002214309789470879.

Souček, O., and Z. Martinec (2008), Iterative improvement of the shallow-ice approximation, *J. Glaciol.*, *54*, 812–822, doi:10.3189/002214308787779924.

Sowers, T., M. Bender, L. Labeyrie, D. Martinson, J. Jouzel, D. Raynaud, J. J. Pichon, and Y. Korotkevich (1993), 135,000 year Vostok-SPECMAP common temporal framework, *Paleoceanography*, *8*, 737–766, doi:10.1029/93PA02328.

Tarasov, L., and W. R. Peltier (2003), Greenland glacial history, borehole constraints, and Eemian extent, *J. Geophys. Res.*, *108*(B3), 2143, doi:10.1029/2001JB001731.

van der Veen, C. J., T. Leftwich, R. von Frese, B. M. Csatho, and J. Li (2007), Subglacial topography and geothermal heat flux: Potential interactions with drainage of the Greenland ice sheet, *Geophys. Res. Lett.*, *34*, L12501, doi:10.1029/2007GL030046.

Watanabe, O., J. Jouzel, S. Johnsen, F. Parrenin, H. Shoji, and N. Yoshida (2003), Homogeneous climate variability across East Antarctica over the past three glacial cycles, *Nature*, *422*, 509–512, doi:10.1038/nature01525.